Article

Cell Reports

Rescue of Metabolic Alterations in AR113Q Skeletal Muscle by Peripheral Androgen Receptor Gene Silencing

Graphical Abstract

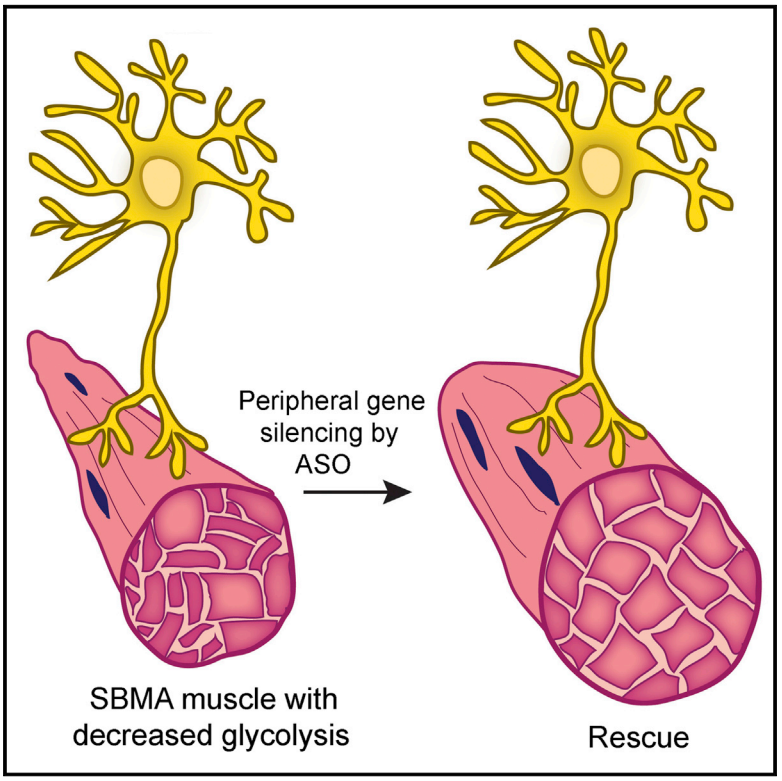

Authors

Elisa Giorgetti, Zhigang Yu, Jason P. Chua, ..., Yuanfang Guan, Gene Hung, Andrew P. Lieberman

Correspondence

liebermn@umich.edu

In Brief

Spinal and bulbar muscular atrophy is a degenerative disorder of the neuromuscular system caused by the polyglutamine androgen receptor (polyQ AR). Giorgetti et al. report that mutant skeletal muscle exhibits alterations in energy metabolism and exercise performance as a consequence of peripheral expression of the polyQ AR.

Highlights

- Decreased expression of carbohydrate metabolic genes characterizes AR113Q muscle
- AR113Q skeletal muscle shows decreased glycolysis and altered mitochondria
- Peripheral gene silencing by ASO rescues expression of muscle energy metabolism genes
- Altered muscle energy utilization contributes to non-neuronal disease manifestations

Accession Numbers

GSE60691

Giorgetti et al., 2016, Cell Reports *17*, 125–136
September 27, 2016
http://dx.doi.org/10.1016/j.celrep.2016.08.084

Cell Reports
Article

Rescue of Metabolic Alterations in AR113Q Skeletal Muscle by Peripheral Androgen Receptor Gene Silencing

Elisa Giorgetti,[1] Zhigang Yu,[1] Jason P. Chua,[1] Ryosuke Shimamura,[1] Lili Zhao,[2] Fan Zhu,[3] Sriram Venneti,[1] Maria Pennuto,[4] Yuanfang Guan,[3] Gene Hung,[5] and Andrew P. Lieberman[1,6,*]
[1]Department of Pathology, University of Michigan Medical School, Ann Arbor, MI 48109, USA
[2]Department of Biostatistics, University of Michigan School of Public Health, Ann Arbor, MI 48109, USA
[3]Department of Computational Medicine and Bioinformatics, University of Michigan Medical School, Ann Arbor, MI 48109, USA
[4]Dulbecco Telethon Institute, Centre for Integrative Biology, University of Trento, Trento 38123, Italy
[5]Ionis Pharmaceuticals, Inc., Carlsbad, CA 92010, USA
[6]Lead Contact
*Correspondence: liebermn@umich.edu
http://dx.doi.org/10.1016/j.celrep.2016.08.084

SUMMARY

Spinal and bulbar muscular atrophy (SBMA), a progressive degenerative disorder, is caused by a CAG/glutamine expansion in the androgen receptor (polyQ AR). Recent studies demonstrate that skeletal muscle is an important site of toxicity that contributes to the SBMA phenotype. Here, we sought to identify critical pathways altered in muscle that underlie disease manifestations in AR113Q mice. This led to the unanticipated identification of gene expression changes affecting regulators of carbohydrate metabolism, similar to those triggered by denervation. AR113Q muscle exhibits diminished glycolysis, altered mitochondria, and an impaired response to exercise. Strikingly, the expression of genes regulating muscle energy metabolism is rescued following peripheral polyQ AR gene silencing by antisense oligonucleotides (ASO), a therapeutic strategy that alleviates disease. Our data establish the occurrence of a metabolic imbalance in SBMA muscle triggered by peripheral expression of the polyQ AR and indicate that alterations in energy utilization contribute to non-neuronal disease manifestations.

INTRODUCTION

The progressive degeneration of the neuromuscular system that occurs in spinal and bulbar muscular atrophy (SBMA) results in skeletal muscle weakness and atrophy and the loss of lower motor neurons in the spinal cord and brainstem (Chua and Lieberman, 2013; Lieberman and Fischbeck, 2000). Clinical onset typically occurs in young to midlife adults and is slowly progressive. The disease is X linked and caused by expansion of a CAG/glutamine tract in the coding region of the first exon of the gene encoding the androgen receptor (AR). Ligand binding to the polyglutamine AR (polyQ AR) promotes nuclear translocation and protein unfolding. Both of these steps are required for pathogenesis and underlie the occurrence of disease only in men (Katsuno et al., 2002; Takeyama et al., 2002). While the polyglutamine tract expansion leads to a partial loss of the AR's transactivation function (Chamberlain et al., 1994; Kazemi-Esfarjani et al., 1995; Lieberman et al., 2002; Mhatre et al., 1993), and this may contribute to features of androgen insensitivity, neuromuscular degeneration is mediated by a toxic gain of function conferred by the misfolded protein. As with all of the polyglutamine disorders, the mechanisms that lead to progressive functional impairment are poorly understood, and disease-modifying therapies are currently unavailable.

Studies of SBMA patients and genetic mouse models have established that skeletal muscle is an important site of toxicity and an attractive therapeutic target. These studies have demonstrated both denervation and myofiber degeneration in muscle biopsies from SBMA subjects (Sorarù et al., 2008). This mixed pathology reflects the occurrence of myopathic symptoms in SBMA patients, including early-onset muscle cramps and elevated levels of serum creatine kinase that exceed those detected in pure denervating diseases (Atsuta et al., 2006; Rhodes et al., 2009). Similarly, analysis of a mouse model of SBMA generated through gene targeting (AR113Q mice) demonstrated the presence of both myopathic and denervating changes in skeletal muscle (Yu et al., 2006a). Highlighting the contribution of skeletal muscle to neuromuscular degeneration are transgenic mice that overexpress the wild-type AR only in muscle and exhibit an SBMA-like phenotype (Johansen et al., 2009; Monks et al., 2007). Similar results have been reported recently in mice overexpressing the polyQ AR only in muscle (Ramzan et al., 2015). Moreover, genetic overexpression of IGF-1 in skeletal muscle alleviates disease in a transgenic mouse model of SBMA (Palazzolo et al., 2009), emphasizing the potential utility of targeting peripheral tissues in this disease. This notion is supported by treatment of AR113Q or polyQ AR bacterial

artificial chromosome (BAC) transgenic mice with subcutaneously (s.c.) administered antisense oligonucleotides (ASOs) targeted against AR (Lieberman et al., 2014). This treatment diminishes polyQ AR expression in the periphery, but not CNS, and rescues disease. These findings are corroborated by genetic studies demonstrating that deletion of a floxed polyQ AR allele only in skeletal muscle prevents disease in BAC transgenic mice (Cortes et al., 2014). Taken together, this body of work has established the importance of polyQ AR expression in skeletal muscle to the SBMA phenotype.

Here, we sought to define critical pathways altered in AR113Q muscle that contribute to the disease phenotype. To accomplish this, we mined gene expression data from skeletal muscle of wild-type and AR113Q males. This approach led to the unanticipated identification of a cohort of genes that regulate carbohydrate metabolism in muscle that are expressed at diminished levels in AR113Q mice. We provide evidence of decreased glycolysis and altered mitochondria in AR113Q muscle and demonstrate that these changes are functionally significant by impacting the response to exercise. Moreover, we establish that subcutaneous administration of ASOs to AR113Q males rescues the expression of diverse genes controlling energy metabolism in muscle. Our data provide evidence of metabolic alterations in SBMA muscle and demonstrate that these changes are triggered by peripheral expression of the polyQ AR.

RESULTS

Decreased Expression of Carbohydrate-Metabolism-Related Genes in AR113Q Muscle

We sought to understand the mechanisms by which expression of the polyQ AR in skeletal muscle contributes to the phenotype of AR113Q knockin mice. To uncover pathways that are altered in disease, we harvested quadriceps muscle from wild-type (WT) and AR113Q males at 14 weeks of age. RNA sequencing (RNA-seq) was used to characterize gene expression, and pairwise analysis uncovered 909 genes differentially expressed by at least 1.5-fold in quadriceps muscle of AR113Q compared to WT mice (Tables S1 and S2). Pathway analysis by Gene Ontology (GO) terms revealed altered expression in AR113Q muscle of regulators of carbohydrate metabolism (Figure 1A). Detailed examination uncovered significantly decreased expression of nine genes encoding enzymes in the glycolytic pathway (Figure 1B). In contrast, none of the genes encoding enzymes in the tricarboxylic acid (TCA) cycle were expressed at significantly different levels in AR113Q muscle. Broad effects on the expression of genes regulating energy metabolism were confirmed in independent cohorts of WT and AR113Q mice by analyzing both a hindlimb muscle (quadriceps) and a pelvic floor muscle that expresses high levels of the polyQ AR (levator ani/bulbocavernosus [LA/BC]). We confirmed by real-time qPCR significantly decreased expression of genes encoding upstream signaling regulators of carbohydrate metabolism (*Prkar2a* and *Prkag3*), and mediators of glucose uptake (*Slc2a4*), glycolysis (*Hk2*), and glycogenolysis (*Phkg1* and *Pygm*) (Figure 1C). Similarly, western blot demonstrated decreased expression of glycolytic enzymes HK2 and GAPDH, but not the mitochondrial respiratory chain component SDHA, in AR113Q muscle (Figure 1D). These data demonstrate an unexpected decrease in the expression of carbohydrate-metabolism-related genes in AR113Q skeletal muscle.

To glean insight into the functional effect of these gene expression changes, WT and AR113Q mice were run on an inclined treadmill for 15 min at increasing speed, and quadriceps muscle was harvested for metabolomics analysis. This intense exercise protocol was designed to favor anaerobic metabolism (Koch and Britton, 2001). Tissues were collected under continuous anesthesia and flash frozen in liquid nitrogen using a procedure that maintains unaltered levels of metabolites in muscle (Overmyer et al., 2015). Samples were analyzed by liquid chromatography-mass spectrometry (LC-MS) and gas chromatography-mass spectrometry (GC-MS). In accordance with gene expression analysis, AR113Q muscle harvested during exercise contained significantly lower levels of the glycolytic intermediates fructose 1,6-bisphosphate (FBP), the product of the rate-limiting and irreversible step in glycolysis, and pyruvate (PYR) (Figures 2A and 2D). A similar trend was detected in levels of 2- and 3-phosphyoglycerate (2PG/3PG), but these did not reach statistical significance because of variability between samples. In contrast, the TCA cycle intermediates citrate/isocitrate (CIT/ICIT), α-ketoglutarate (AKG), fumarate (FUM), and malate (MAL) were unchanged between cohorts (Figures 2B and 2D). These data are indicative of a more severe functional impairment of glycolysis than the TCA cycle and are consistent with the broad decrease in expression of carbohydrate-metabolism-related genes in AR113Q muscle (Figure 1). Metabolomics additionally identified significantly diminished levels of NAD and NADP in AR113Q muscle, findings that are suggestive of lower metabolism through the glycolytic pathway (Figure 2C). In contrast, no difference in levels of ATP was observed (Figure 2C), consistent with the notion that the TCA cycle was relatively intact in mutant muscle.

Mitochondrial Defects in AR113Q Skeletal Muscle

We next sought to establish the extent to which mitochondrial abnormalities accompanied alterations in the expression of carbohydrate-metabolism-related genes in AR113 muscle. Prior studies identified mitochondrial defects in cellular models of SBMA and showed diminished expression of several mitochondrial genes in AR113Q muscle (Ranganathan et al., 2009). We performed transmission electron microscopy (TEM) on WT and AR113Q soleus muscles (Figure 3A). The soleus is rich in slow-twitch oxidative fibers that contain a large number of mitochondria. While sarcomere architecture was intact in mutants, we observed a significant decrease in the mean area occupied by intermyfibrillar mitochondria (Figures 3A and 3B). Similarly, mtDNA copy number was significantly decreased in the LA/BC (Figure 3C). Moreover, ~20% of mitochondria in AR113Q muscle were either focally swollen or tightly associated with vesicles, many of which resembled autophagosomes (Figures 3A, 3D, and S1). This finding is consistent with the robust activation of macroautophagy previously demonstrated in AR113Q skeletal muscle (Chua et al., 2014; Yu et al., 2011) and suggests the occurrence of increased mitophagy. To test functional status, mitochondria were isolated from WT or AR113Q muscle for Seahorse analysis. Mitochondria from quadriceps muscles of

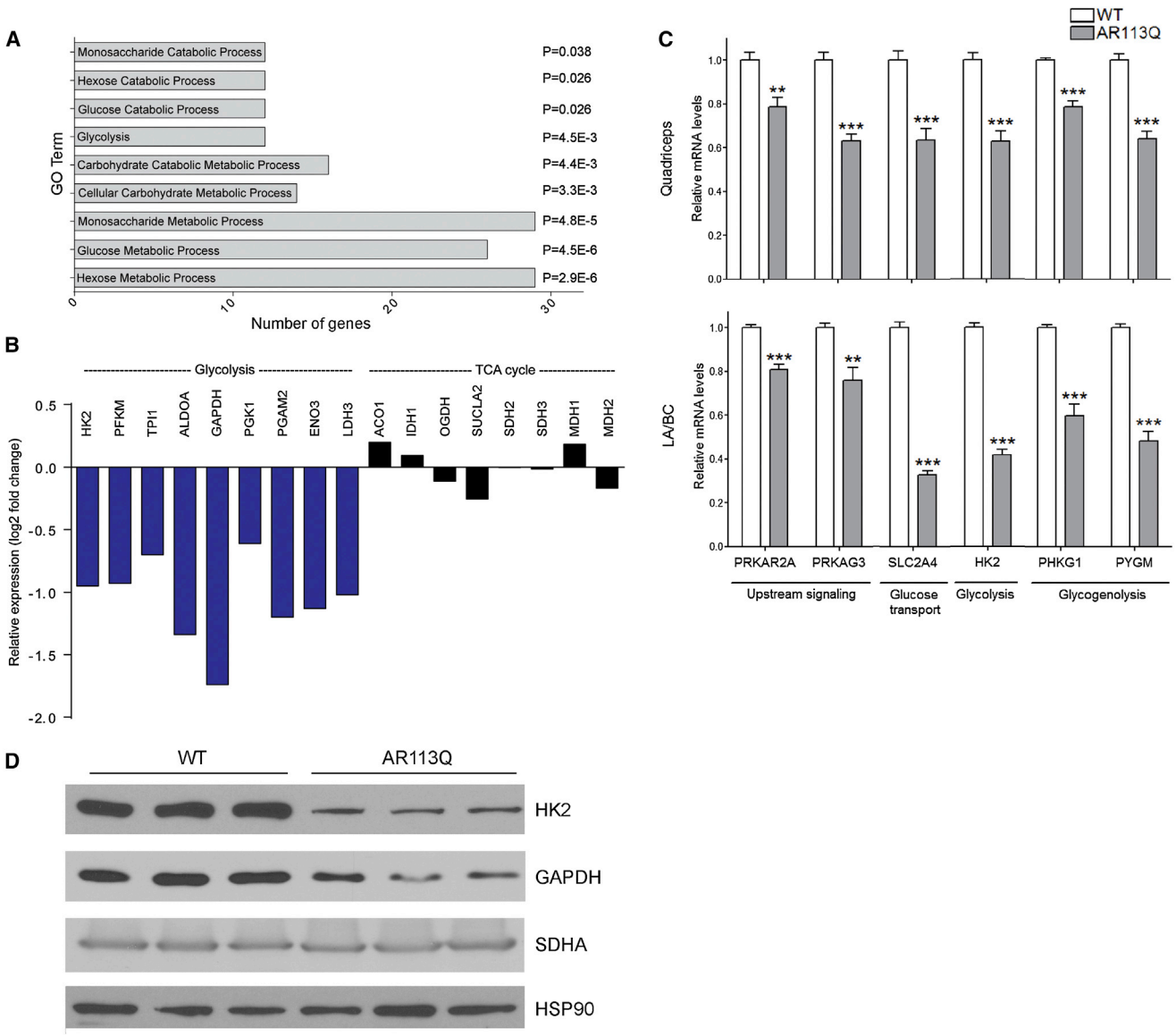

Figure 1. Decreased Expression of Carbohydrate Metabolism Genes in AR113Q Skeletal Muscle

(A and B) Quadriceps muscles from wild-type (WT) or AR11Q males (n = 3/group) were harvested at 14 weeks of age and gene expression was analyzed by RNA-seq. (A) GO terms of differentially expressed genes ($\geq$1.5-fold) related to carbohydrate metabolism. p values by false discovery rate are indicated.

(B) Relative expression of genes encoding glycolytic or TCA cycle enzymes in AR113Q versus WT muscle. Shown in blue are genes whose expression is changed by $\geq$1.5-fold and in black genes whose expression is changed by <1.5-fold.

(C) Expression of carbohydrate metabolism-related genes in quadriceps and LA/BC muscles of WT and AR113Q mice (mean ± SEM; n = 5/group). **p < 0.01; ***p < 0.001 by Student's t test.

(D) Western blots of HK2, GAPDH, and SDHA in lysates from LA/BC muscles of WT and AR113Q mice.

AR113Q mice were significantly more uncoupled than those from WT mice (Figure 3E). These findings suggest that a fraction of mitochondria in AR113Q muscle are dysfunctional.

Altered Response of AR113Q Mice to Exercise

Our observations of altered carbohydrate-metabolism-related gene expression and mitochondrial abnormalities led us to compare metabolic rate and substrate utilization in WT and AR113Q mice. Oxygen consumption (VO_2, mg/kg/hr) and energy expenditure (kcal/kg/hr) were quantified by CLAMS (the Comprehensive Laboratory Animal Monitoring System) analysis for three consecutive days. No significant differences in energy metabolism during home cage activity were detected between the two groups (Figure 4A). Similarly, serum glucose and insulin levels as measured during a glucose tolerance test were unchanged in AR113Q males (Figure S2). However, when mice were challenged to perform acute exercise, significant differences between these cohorts emerged (Figure 4B). Mice were

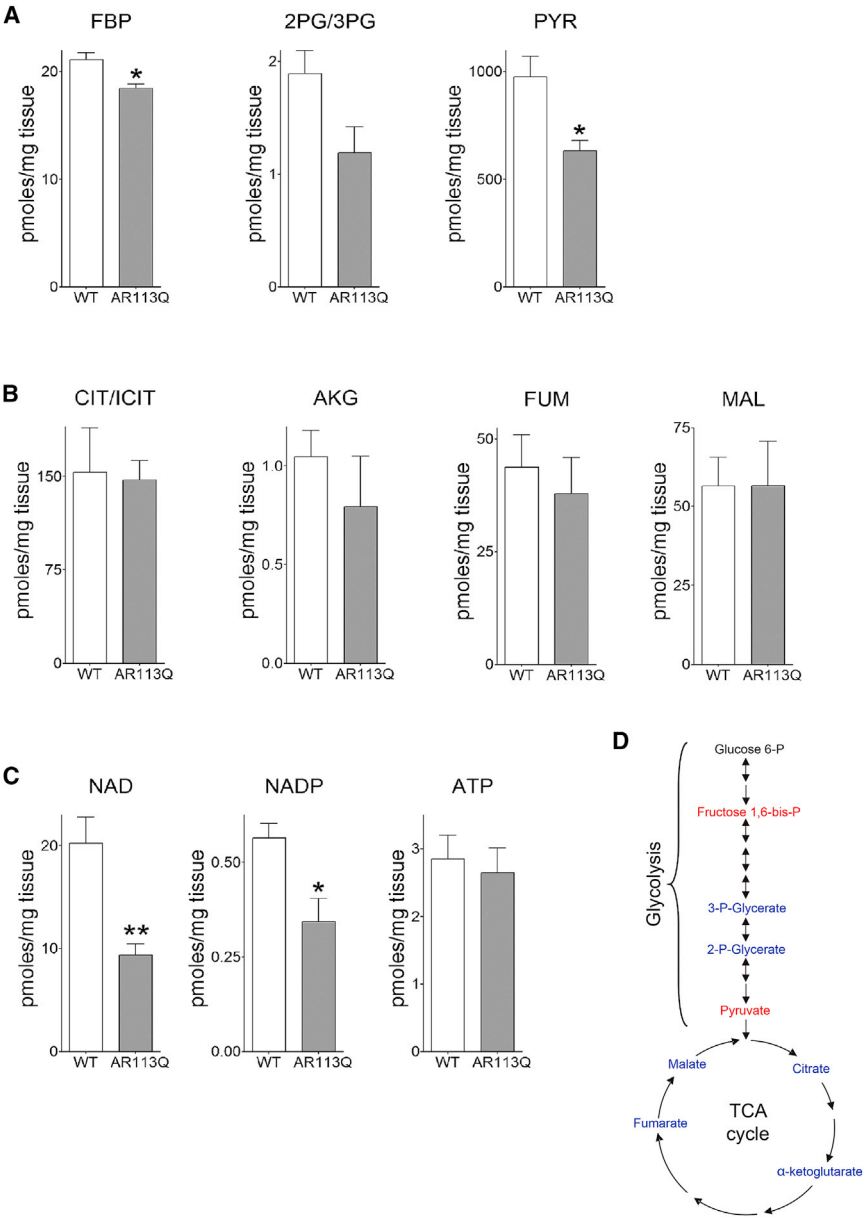

Figure 2. Energy Metabolites in Skeletal Muscle during Exercise

WT and AR113Q male mice at 14 weeks were run at increasing speeds on an inclined treadmill for 15 min, and quadriceps muscles were then harvested for analysis.

(A) Glycolytic metabolites fructose 1,6-bis-P (FBP), 2- and 3-phosphyglycerate (2PG/3PG), and pyruvate (PYR).

(B) TCA cycle metabolites citrate/isocitrate (CIT/ICIT), α-ketoglutarate (AKG), fumarate (FUM), and malate (MAL).

(C) NAD, NADP, and ATP levels (mean ± SEM; n = 4/group). *p < 0.05; **p < 0.01 by Student's t test.

(D) Schematic highlighting measured glycolytic and TCA cycle metabolites. Metabolites significantly different between WT and AR113Q are in red, unchanged in blue, and not measured in black.

tasked to run on an inclined treadmill at increasing speeds for 30 min or until exhaustion. While both groups of mice ran the same time and distance, AR113Q mice expended more energy and consumed more oxygen to complete this task. These differences were consistent with partial mitochondrial uncoupling in AR113Q muscle (Figure 3E), and may reflect enhanced utilization of fats or amino acids as alternative energy sources to carbohydrates.

The metabolic alterations in AR113Q muscle after intense, acute exercise prompted us to determine whether mutant males would respond aberrantly to modest, chronic exercise. To test this possibility, WT and AR113Q males were randomly assigned to exercise or rest cohorts, with exercise cohorts completing a mild running regimen from 8 to 14 weeks of age. Mice were run 5 days per week on a horizontal treadmill for 30 min at 10 m/minute, while control mice were placed on the immobile apparatus for the same duration to control for confounding effects from environmental enrichment. This low-intensity endurance exercise protocol was designed to favor oxidative metabolism. All WT mice completed the 6 weeks of training, while only seven out of ten AR113Q mice in the exercise cohort (70%) and six out of eight AR113Q mice in the rest cohort (75%) survived until the end of the study (Figure 5A). This is consistent with previous analysis of lifespan in AR113Q mice (Yu et al., 2006a) and indicates that exercise did not impact survival. While chronic exercise significantly improved forelimb grip strength of WT males, it had no effect on AR113Q mice (Figure 5B). Moreover, analysis of soleus and gastrocnemius muscles showed that both type I and type II fibers were significantly reduced in size in exercised AR113Q mice, whereas WT muscle showed the opposite effect (Figures 5C and 5D). Notably, exercise did not alter polyQ AR protein levels or aggregation in mutant muscle (Figure S3). These data demonstrate an aberrant response to chronic, low-intensity exercise in AR113Q males.

Peripheral polyQ AR Gene Suppression Rescues Expression of Muscle Metabolism Genes

We hypothesized that peripheral expression of the polyQ AR contributed to altered expression of carbohydrate metabolism-related genes in AR113Q muscle. This notion was based on recent studies demonstrating that subcutaneous administration of *Ar*-targeted ASO decreases expression of the mutant protein in skeletal muscle, but not in spinal cord, and ameliorates

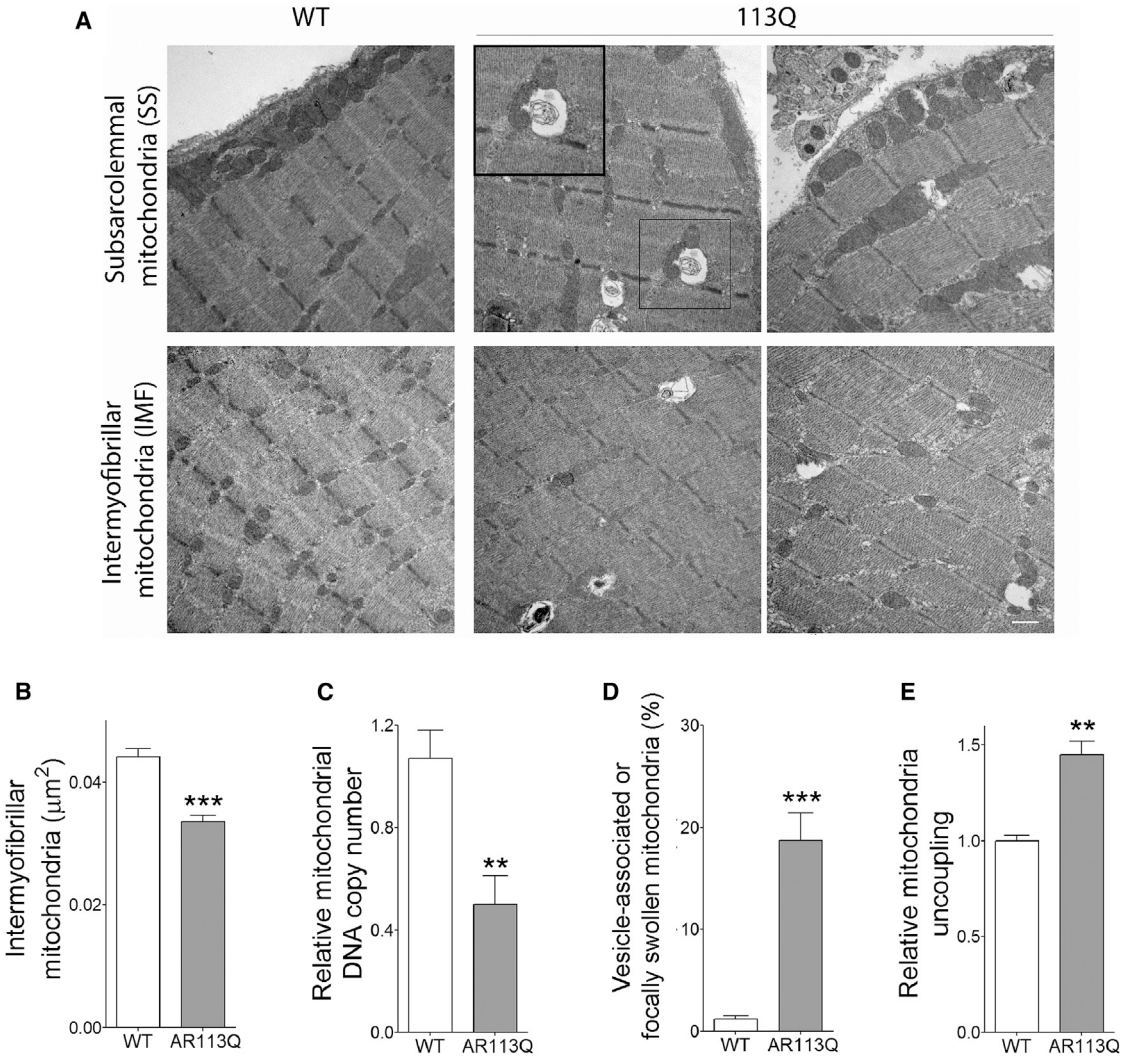

Figure 3. Mitochondrial Defects in the Skeletal Muscle of AR113Q Mice

(A) Representative TEMs of soleus muscle from WT and AR113Q males at 14 weeks. Inset shows vesicle-associated mitochondria. Scale bar, 500 nm.

(B) Mean area ± SEM of intermyofibrillar mitochondria (n = 3 mice/group; ≥90 mitochondria/mouse). ***p < 0.001 by Student's t test.

(C) mtDNA copy number in the LA/BC muscle of WT and AR113Q mice measured as a ratio between mtDNA (D loop) and genomic DNA (β2 m) (mean ± SEM; n = 8/group). **p < 0.01 by Student's t test.

(D) Percentage of mitochondrial with focal swellings or associated with vesicles (mean ± SEM; n = 3/group; ≥90 mitochondria per mouse). ***p < 0.001 by Student's t test.

(E) Relative uncoupling of mitochondria isolated from quadriceps muscles of WT and AR113Q mice (mean ± SEM; n = 3/group). **p < 0.01 by Student's t test.

disease (Lieberman et al., 2014). To test this hypothesis, AR113Q males received a therapeutic dose of *Ar*-targeted ASO (50 mg/kg per week, s.c.) from 6 to 14 weeks of age. Quadriceps muscles were harvested and gene expression determined by RNA-seq. This analysis demonstrated that nearly three-quarters of the gene expression differences detected in the comparison of AR113Q versus WT muscle were rescued by peripheral treatment with ASO (Figure 6A; Tables S1 and S3). As this intervention alleviates the disease phenotype, we focused on the 666 genes whose expression was responsive to ASO administration. Analysis of GO terms demonstrated that many of the carbohydrate metabolism-related genes whose expression was altered in AR113Q muscle were rescued by ASO treatment (Figure 6B). Notably, of the 21 ASO-responsive genes identified in the GO term "hexose metabolic process," 19 were expressed at lower levels in AR113Q muscle. Moreover, one of the genes expressed at higher levels in mutant muscle was *Cpt1a,* encoding a protein that is essential for uptake of long-chain fatty acids into mitochondria. In addition, of the nine genes encoding glycolytic enzymes that were expressed at lower levels in AR113Q muscle (Figure 1B), all except *Gapdh* and *Pgk1* were rescued by treatment with ASO (Tables S1, S2). We confirmed that treatment with *Ar*-targeted ASO, but not a non-targeted control, diminished expression of AR mRNA and rescued the expression

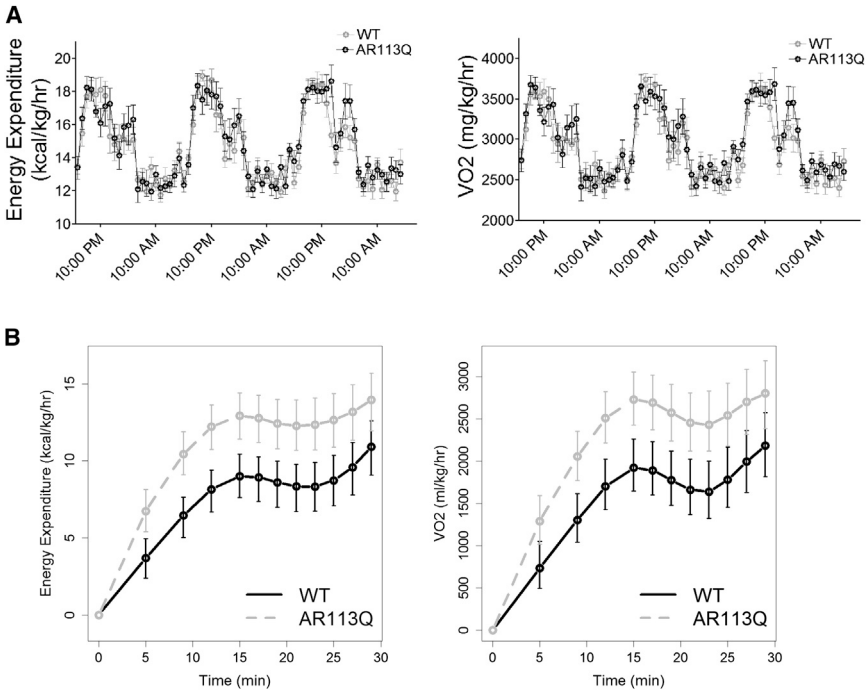

Figure 4. Enhanced Energy Expenditure and Oxygen Consumption in AR113Q Mice during Exercise

(A) Home-cage energy expenditure (kcal/kg/hr) and O_2 consumption (mg/kg/hr) in WT and AR113Q mice at 14 weeks, as measured during three consecutive days (mean ± SEM; n = 9/group).

(B) Energy expenditure (kcal/kg/hr) and O_2 consumption (mg/kg/hr) in WT and AR113Q mice during acute running at increasing speeds on an inclined treadmill (mean ± SEM; n = 9/group). *p < 0.05 for all time points from 5 to 25 min.

of carbohydrate metabolism-related genes in skeletal muscle (Figure 6C). In addition, we identified ASO-responsive expression of a limited set of mitochondria-related genes including *Ppargc1b* (peroxisome proliferator-activated receptor gamma, coactivator 1 beta [PGC-1β]), a transcriptional co-activator of genes regulating mitochondrial function (Villena, 2015), and *Bbc3* (BCL2 binding component 3), a BCL-2 family member that induces mitochondrial outer membrane permeabilization (Huang and Strasser, 2000) (Figure 6D).

Altered Expression of Upstream Regulators of Energy Homeostasis

Given the large number of genes related to carbohydrate metabolism whose expression was diminished in AR113Q muscle, we reasoned that activity of upstream regulators of this pathway might be altered. To explore this possibility, we analyzed the set of ASO-responsive genes identified through RNA-seq by Ingenuity Pathway Analysis (IPA). This analysis identified several interrelated nodes of canonical pathways and upstream regulators that converge to influence energy homeostasis (Figure 7A). Among these pathways were genes associated with protein kinase A (PKA) (*Prkar2a*; $p = 4.51 \times 10^{-6}$) (Table S3) and AMPK (5′ AMP-activated protein kinase) signaling, including the γ3 regulatory subunit of AMPK (*Prkag3*; $p = 7.72 \times 10^{-14}$). In skeletal muscle, AMPK regulates glucose transport as well as mitochondrial function and biogenesis (reviewed in Lantier et al., 2014). IPA also identified transcription factors SRF (serum response factor) ($p = 7.55 \times 10^{-12}$) and NR4A1 (nuclear receptor subfamily 4, group A, member 1) ($p = 9.18 \times 10^{-13}$). NR4A1 is an orphan receptor in the steroid-thyroid hormone-retinoid receptor superfamily that is induced by diverse stimuli in skeletal muscle, including PKA signaling (Kanzleiter et al., 2009; Maxwell et al., 2005), as well as the transcription factor SRF (Iacono et al., 2013; Jin et al., 2011). As NR4A1 regulates skeletal muscle expression of genes influencing glucose transport, insulin signaling, glycolysis, and glycogenolysis (Chao et al., 2007, 2009; Kanzleiter et al., 2010; Maxwell et al., 2005), we sought to confirm its altered expression in AR113Q muscle. Significantly decreased expression of NR4A1 mRNA was found in AR113Q versus WT quadriceps, and this defect was rescued by treatment with *Ar*-targeted, but not control, ASO (Figure 7B). In contrast, no changes in the expression of genes encoding NR4A1 or HK2 were detected in spinal cord of AR113Q mice (Figure S4), indicating that altered expression of carbohydrate-metabolism-related genes was a phenotype more robustly manifest by skeletal muscle. Analysis of RNA-seq data indicated that 17 genes reported to respond to alterations in NR4A1 expression (Pearen and Muscat, 2010) were differentially expressed in AR113Q versus WT quadriceps (Tables S1 and S4), suggesting that the activity of this transcription factor was decreased in mutant muscle. Notably, the majority of these genes encoded proteins involved in carbohydrate metabolism, and the expression of 13 of them was restored by ASO treatment.

Prior studies have demonstrated that expression of NR4A1 is significantly reduced in skeletal muscle after denervation (Chao et al., 2007). We confirmed this observation in gastrocnemius muscle of WT mice following sciatic nerve transection and additionally demonstrated decreased expression of the NR4A1-responsive genes *Scl2a4* and *Phkg1* (Figure 7C). As these genes were also downregulated in AR113Q muscle and restored by ASO, we conclude that peripheral polyQ AR induces changes in muscle that mimic those triggered by denervation to influence the expression of metabolic genes. This likely reflects an underlying impairment of communication between skeletal muscle and innervating motor neurons that influences the expression of regulators of skeletal muscle energy metabolism and the response to exercise in AR113Q mice.

DISCUSSION

We demonstrate previously unrecognized alterations in skeletal muscle energy metabolism that are a consequence of peripheral

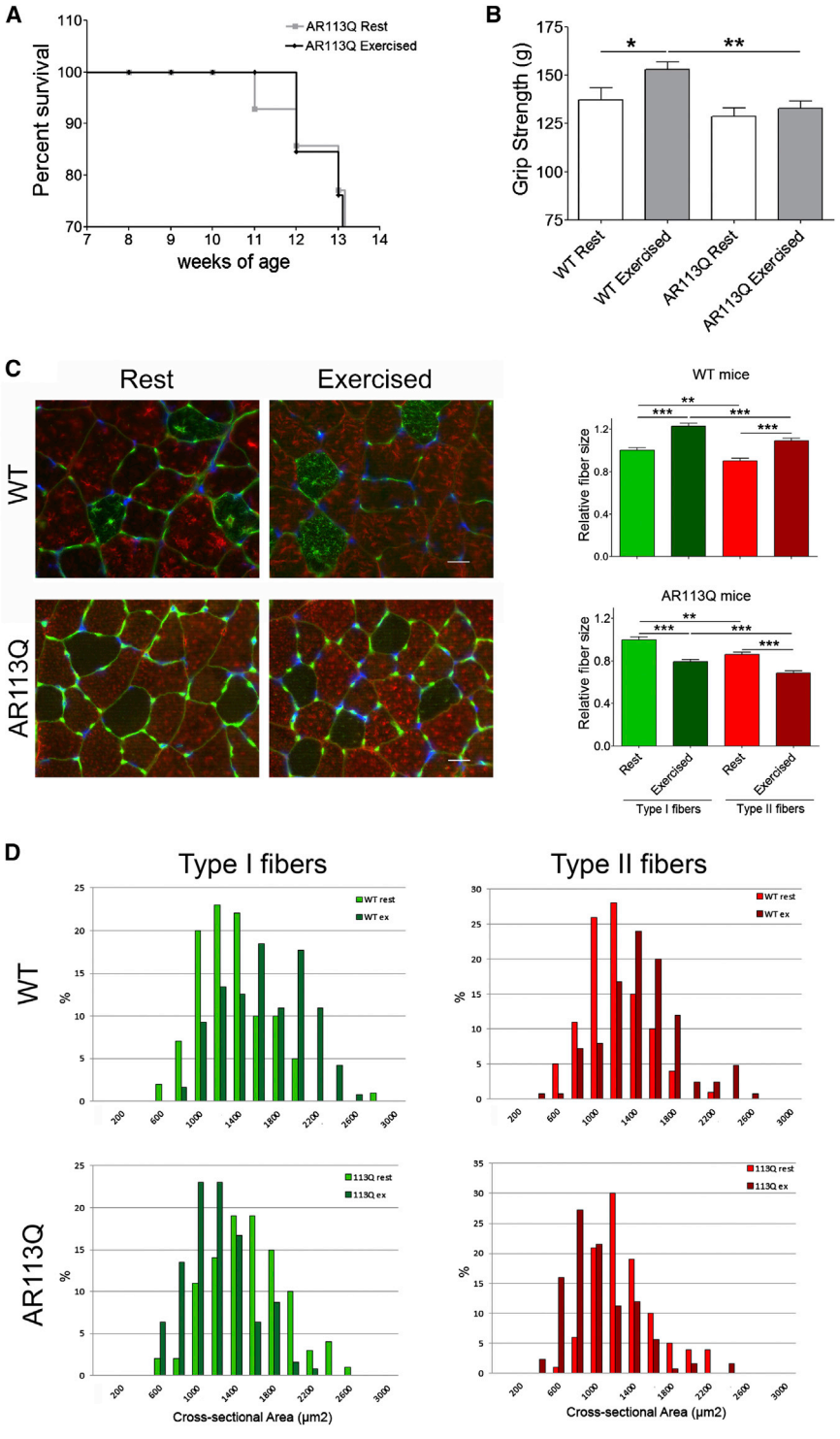

Figure 5. Effects of Chronic Exercise in AR113Q Mice

WT and AR113Q mice were run on a treadmill five times per week for 30 min at 10 m/minute for 6 weeks, from 8 to 14 weeks of age. Control mice ("rest") were placed on an immobile treadmill apparatus for an equivalent time.

(A) Survival of AR113Q males was not altered by exercise. $p > 0.05$ by log-rank analysis.

(B) Forelimb grip strength (g) of WT and AR113Q mice assessed at the end of the 6-week training period (mean ± SEM; $n \geq 4$ WT mice/group; $n \geq 6$ AR113Q mice/group). *$p < 0.05$; **$p < 0.01$ by one-way ANOVA.

(C) Left: immunofluorescence staining for type I slow-twitch heavy-chain myosin (green) and type II fast-twitch heavy-chain myosin (red) in soleus/gastrocnemius muscles. Basement membrane was stained with wheat germ agglutinin (green); nuclei were stained by DAPI (blue). Scale bar, 20 μm. Right: relative mean fiber size ± SEM; $n \geq 4$ mice/group, ≥ 25 fibers/mouse. **$p < 0.01$, ***$p < 0.001$ by one-way ANOVA.

(D) Fiber size distribution of type I and type II fibers in WT and AR113Q mice ($n \geq 4$ mice/group, ≥ 25 fibers/mouse).

polyQ AR expression (Figure S5). RNA-seq data led to the discovery of decreased expression of numerous genes regulating carbohydrate metabolism in skeletal muscle of mutant males. These changes are accompanied by evidence of diminished activity of regulators of glucose utilization, including upstream signaling pathways controlled by PKA and AMPK and downstream transcription factors such as SRF and NR4A1. We suggest that diminished energy utilization through glycolysis leads to a shift toward alternative energy sources such as lipids and that this contributes to mitochondrial damage and dysfunction. The consequences of these metabolic alterations are evident during intense, acute exercise that favors anaerobic metabolism and following chronic, low-intensity endurance exercise that favors oxidative metabolism.

Interestingly, we note that similar alterations in gene expression occur following sciatic nerve transection in WT mice. Our observations are consistent with prior reports indicating that loss of β-adrenergic signaling following denervation contributes to diminished PKA activity and reduced expression of NR4A1 and its target genes (Chao et al., 2007). Metabolic alterations characterized by a glycolytic to oxidative shift also occur in skeletal muscle of transgenic mice expressing mutant G86R SOD1 (Palamiuc et al., 2015), and clinical studies have demonstrated that approximately two-thirds of patients with amyotrophic lateral sclerosis are hypermetabolic (Desport et al., 2005). These findings support the concept that muscle energy metabolism is altered in degenerative motor neuron

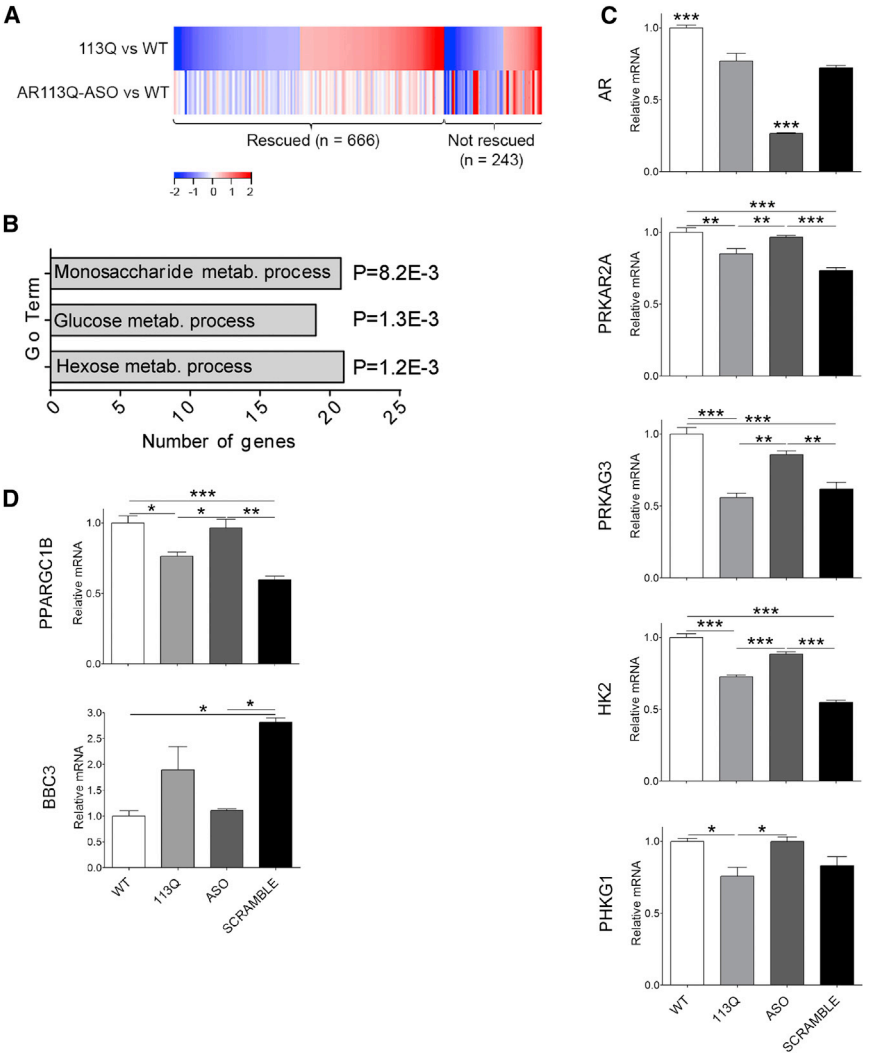

Figure 6. Peripheral ASO Treatment Rescues Expression of Metabolic Genes in AR113Q Muscle

Male mice (n = 3/group) were treated with ASO (50 mg/kg per week, s.c.) or vehicle from 6 to 14 weeks of age, and gene expression in skeletal muscle was analyzed by RNA-seq.

(A) Heatmap shows genes differentially expressed (≥1.5-fold) in quadriceps muscle of AR113Q versus wild-type (WT) mice (top row). Differential expression in ASO-treated AR113Q versus WT muscle (bottom row) highlights genes rescued by ASO (expression difference <1.5-fold). Activated genes are shown in red and repressed genes in blue.

(B) GO terms of differentially expressed genes (≥1.5-fold) related to carbohydrate metabolism that are rescued by treatment with ASO. p values by false discovery rate are indicated.

(C and D) Relative mRNA levels in quadriceps muscle of WT, AR113Q, and AR113Q mice treated with AR-targeted ASO or control ASO (SCRAMBLE) from 6 to 14 weeks of age (mean ± SEM; n = 3/group). *p < 0.05; **p < 0.01; ***p < 0.001 by one-way ANOVA. Expression of AR and carbohydrate metabolism-related genes (C) and mitochondrial-related genes (D) is shown.

diseases as a consequence of denervation. Our data indicate that similar changes occur in AR113Q mice due to peripheral expression of the polyQ AR. The identification of ASO-sensitive changes in the expression of carbohydrate metabolism genes complements previously characterized changes in markers of denervation, including acetylcholine receptor-α subunit and myogenin mRNAs, that are also abnormal in AR113Q muscle and rescued by peripheral gene knockdown (Lieberman et al., 2014). Taken together, these findings indicate that peripherally expressed polyQ AR disrupts communication between motor neurons and skeletal muscle and recapitulates gene expression and metabolic alterations in skeletal muscle that have been previously characterized to occur following injury to motor neurons or their axons. Prior studies have demonstrated impaired retrograde labeling of spinal motor neurons in AR113Q mice despite the absence of morphological abnormalities at the neuromuscular junction that are evident by light microscopy (Kemp et al., 2011), suggesting that disruption of nerve-muscle communication may initially reflect functional, rather than structural changes.

The model of pathogenesis that we present (Figure S5) places alterations in carbohydrate metabolism upstream of the mitochondrial abnormalities that were identified in AR113Q muscle, including diminished mitochondrial number, increased mitophagy, and partial mitochondrial uncoupling. This latter effect may be a consequence of damage by reactive oxygen species (Mailloux and Harper, 2012), perhaps arising due to the use of fats as an important, alternative energy source. This model is based on gene expression analysis that showed a large number of changes involving regulators of glucose metabolism compared to components of the TCA cycle and metabolomics analysis that showed significantly lower levels of glycolytic intermediates without alterations in TCA cycle metabolites. We note that it is also possible that the polyQ AR may directly damage mitochondria, as previously suggested (Ranganathan et al., 2009), and that in this setting, alterations in glycolysis may occur secondary to mitochondrial damage. Indeed, it is possible that both pathways are directly targeted by the polyQ AR. Further analysis to clarify the relationship between changes in glycolysis and mitochondria in SBMA muscle will be an important focus of future studies.

The occurrence of metabolic abnormalities in AR113Q muscle underlying an impaired response to exercise suggests that these changes are important aspects of the neuromuscular phenotype of SBMA patients. Indeed, a recent report showed decreased levels of HK2, PFKFB3, and GAPDH mRNA in skeletal muscle from SBMA patients, accompanied by a glycolytic to oxidative

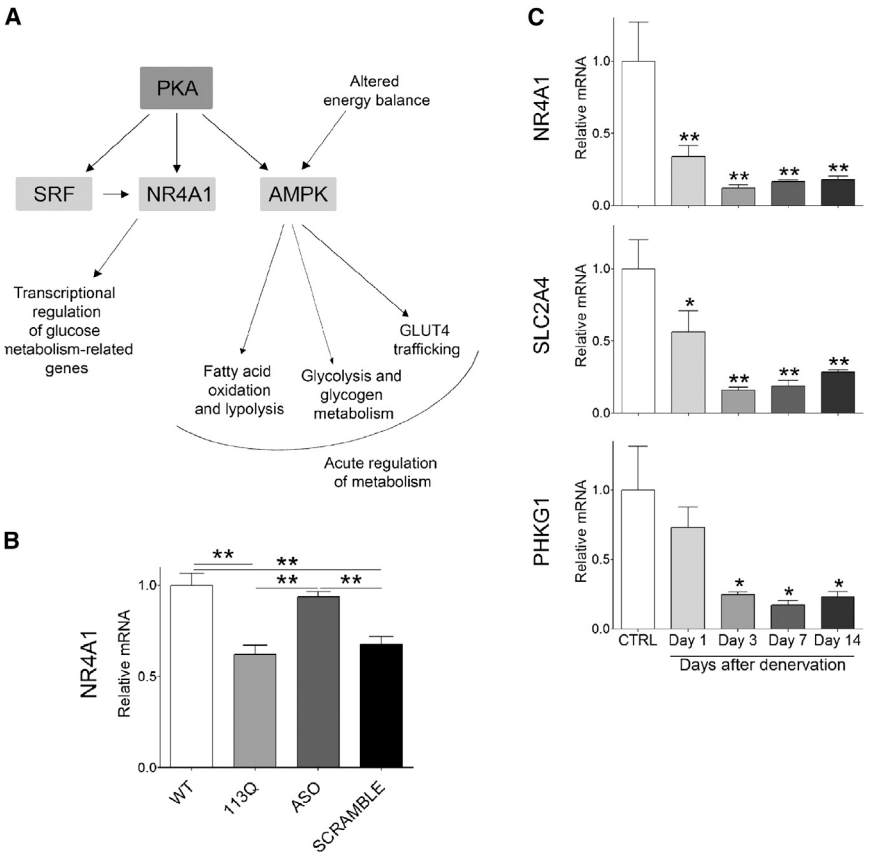

Figure 7. Regulators of Energy Metabolism Are Sensitive to Peripheral polyQ AR Expression

(A) Gene clusters identified through Ingenuity Pathway Analysis. Canonical pathways are shown in dark gray and upstream regulators in light gray.

(B) NR4A1 mRNA levels in quadriceps muscle of WT, AR113Q, and AR113Q mice treated with AR-targeted ASO or control ASO (SCRAMBLE) from 6 to 14 weeks of age (mean ± SEM; n = 3/group). **p < 0.01 by one-way ANOVA.

(C) Expression of NR4A1 and target genes that regulate carbohydrate metabolism in gastrocnemius muscles of control WT male mice following sciatic nerve transection (mean ± SEM; n = 3/group). *p < 0.05; **p < 0.01 by one-way ANOVA.

shift in muscle fibers (Rocchi et al., 2016). These alterations may have contributed to the modest effects of exercise observed in a randomized study of SBMA patients (Shrader et al., 2015) and in the poor tolerance of SBMA patients to aerobic exercise in an observational study (Dahlqvist and Vissing, 2016). Moreover, skeletal muscle plays a critical role in energy homeostasis for the organism, accounting for ~25% of energy expenditure in the resting state. As such, altered energy utilization by skeletal muscle may play a part in the systemic manifestations of disease. Recent studies have demonstrated elevated fasting glucose as well as increased total cholesterol, low-density lipoprotein cholesterol, and triglyceride levels in a cohort of SBMA patients (Querin et al., 2016). These findings add to a growing appreciation of non-neuronal phenotypes in this disorder and raise the possibility that targeting metabolic alterations may alleviate disease manifestations. In support of this hypothesis is recent work demonstrating that feeding mice a high-fat diet diminishes aspects of the SBMA phenotype (Rocchi et al., 2016). Additional evidence suggests that enhancing anabolic support of muscle is also beneficial in SBMA mice. Abrogation of SUMO modification of the polyQ AR enhances its activity as a ligand-dependent transcription factor, increases the expression of genes related to mitochondria function in skeletal muscle, and rescues both exercise endurance and type I muscle fiber atrophy in mutant mice (Chua et al., 2015).

Derangements of energy utilization and homeostasis have emerged as important components of the pathophysiology of many age-dependent neurodegenerative disorders and of aging itself. The changes documented here in AR113Q skeletal muscle indicate that similar processes occur in SBMA. Moreover, our analysis suggests that these changes arise due to expression of the polyQ AR in muscle and demonstrates that they are mitigated by peripherally targeted therapies. The extent to which similar metabolic alterations also impair function of lower motor neurons in SBMA patients remains to be more fully explored, although our initial analysis of AR113Q mice suggests less severe gene expression changes in spinal cord than in skeletal muscle. As such, we speculate that targeting the metabolic phenotype trigged by expression of the polyQ AR may be particularly effective in rescuing non-neuronal manifestations of the disease, including important aspects of skeletal muscle dysfunction.

EXPERIMENTAL PROCEDURES

Mice

Gene-targeted mice with an *Ar* allele containing 113 CAG repeats (AR113Q mice) were previously described (Yu et al., 2006a, 2006b). Mice were group housed in a specific-pathogen-free (SPF) facility, provided with chow and water ad libitum, and maintained on a constant 12-hr light/12-hr dark cycle. Genotypes were verified by PCR of DNA harvested from tail biopsy specimens obtained shortly after weaning, using the forward primer 5′-CCAGAA TCTGTTCCAGAGCGTG-3′ and the reverse primer 5′-TGTTCCCCTGGACT CAGATG-3′.

ASO Treatment

AR113Q male mice and WT littermates were treated for 8 weeks with ASOs. The 16-mer, 2′,4′-constrained ethyl gapmer ASO complementary to human and mouse *AR* transcripts and the 20-mer control have been described previously (Lieberman et al., 2014). Subcutaneous administration of 50 mg/kg body weight of *AR*-targeted ASO (ASO1 from ref) or control ASO (SCRAMBLE; control ASO from ref) was performed once a week from 6 to 14 weeks of age (n = 3 per group). Quadriceps muscle was harvested at 14 weeks for analysis of mRNA expression.

Sciatic Nerve Transection

C57BL/6J male mice at 7 weeks of age were used for studies of denervated muscle as detailed in the Supplemental Experimental Procedures.

All procedures involving mice were approved by the University of Michigan Committee on Use and Care of Animals, in accord with the NIH Guidelines for the Care and Use of Experimental Animals.

Gene Expression

Total RNA was isolated from quadriceps and LA/BC muscles with TRIzol Reagent (Life Technologies) according to the manufacturer's instructions. RNA (1 μg) was reverse transcribed to cDNA using the High Capacity cDNA Reverse Transcription Kit (Applied Biosystems). Gene-specific primers with FAM-labeled probes were from Applied Biosystems: Nr4a1, *Mm01300401_m1*; Prkar2a, *Mm00435916_m1*; Prkag3, *Mm00463997_m1*; Hk2, *Mm00443385_m1*; Slc2a4, *Mm01245502_m1*; Phkg1, *Mm02580948_m1*; Pygm, *Mm00478582_m1*; Ppargc1a, *Mm01208835_m1*; Ppargc1b, *Mm00504720_m1*; Bbc3, *Mm00519268_m1*. AR-specific forward primer 5′-CCAGTCCCAATTGTGT CAAA-3′ and reverse primer 5′-TCCCTGGTACTGTCCAAACG-3′ (Life Technologies) were used with Roche Universal Probe Library FAM-labeled probe #58 (catalog number 04688554001). Cpsf2-specific primers with VIC-labeled probes (Applied Biosystems; *Mm00489754_m1*) were used as internal control. qPCR was carried out using FastStart TaqMan Probe Master Mix (Roche) on software supplied with a 7500 Real-Time PCR SDS System (Applied Biosystems). PCR cycling conditions were as follows: 50°C for 2 min, 95°C for 10 min, 40 cycles at 95°C for 15 s, and 60°C for 1 min.

RNA-Seq Data

For RNA-seq, cDNA was prepared into sequencer-ready fragment libraries using the Illumina TruSeq mRNA-Seq Sample Prep Kit according to manufacturer's protocols, and sequenced on the Illumina HiSeq 2000 using manufacturer's protocols for paired-end, 100-nt sequencing. Samples were multiplexed into pools of six samples each, and each pool was sequenced on one lane of the sequencer. The software package Tuxedo Suite was used for alignment, differential expression analysis, and postanalysis diagnostics (Langmead et al., 2009; Trapnell et al., 2009, 2013). The reference transcriptome (UCSC mm10) (http://genome.ucsc.edu/) was used for alignment. Expression quantitation and differential expression analysis were performed using CuffDiff (Cufflinks version 2.1.1). Genes and transcripts were identified as differentially expressed based on three criteria: test status = OK, false discovery rate (FDR) < 0.05, and fold change ≥ 1.5. Analysis of differentially expressed genes to identify significantly enriched functional categories was performed using DAVID and IPA (QIAGEN). The heatmap was plotted in R using the gplots and RcolorBrewer packages.

Transmission Electron Microscopy

Mice were perfused with 2.5% glutaraldehyde in 0.1 M phosphate buffer (pH 7.4), and soleus muscle was collected. Ultra-thin tissue sections were obtained with a diamond knife, placed on copper grids, and stained with uranyl acetate and lead citrate. Image acquisition was performed with a Philips CM-100 transmission electron microscope. Total mitochondria number and vesicle-associated mitochondria were manually counted (n = 3 mice/group, ≥500 mitochondria/group). Mitochondria area (μm^2) was measured by ImageJ software (n = 3 mice/group, ≥250 mitochondria/group).

mtDNA Copy Number

Genomic and mtDNA was isolated from LA/BC using the QIAamp DNA Micro Kit (QIAGEN). *D loop* forward primer 5′-GACCAACATAACTGTGGTGTCA-3′ and reverse primer 5′-ATTCTTCTCCGTAGGTGCGTCTAG-3′ were designed to quantify mtDNA; *Beta-2 microglobulin* (B2m) forward primer 5′-TGTCAGA TATGTCCTTCAGCAAGG-3′ and reverse primer 5′-TGCTTAACTCTGCAG GCGTATG-3′ were designed to quantify genomic DNA as an internal control. qPCR was carried out using SYBR Select Master mix (Life Technologies) on software supplied with a 7500 Real-Time PCR SDS System (Applied Biosystems). PCR cycling conditions were as follows: 50°C for 2 min, 95°C for 10 min, 40 cycles at 95°C for 15 s, and 60°C for 1 min. Data were expressed as Ct values and used for the relative quantification of targets with the ΔΔCt calculation to give N-fold differences. Data were transformed through the equation $2^{-\Delta\Delta Ct}$.

Mitochondria Uncoupling

Mitochondria were isolated from quadriceps muscles of WT and AR113Q mice, and uncoupling was assessed as detailed in the Supplemental Experimental Procedures.

CLAMS and Glucose Tolerance Test

Oxygen consumption (VO_2), carbon dioxide production (VCO_2), spontaneous motor activity, and food intake were measured using CLAMS (Columbus Instruments), an integrated open-circuit calorimeter equipped with an optical beam activity monitor. This analysis and glucose tolerance testing was performed by the University of Michigan Metabolomics Core and is described in detail in the Supplemental Experimental Procedures.

Metabolomics

WT and AR113Q male mice ran on an Exer3/6 treadmill (Columbus Instruments) with 25°C slope for 15 min at increasing speeds (as described for CLAMS analysis). Animals were induced into anesthesia at a dose of 5% isoflurane and then maintained by continuous inhalation of 2% isoflurane. Quadriceps muscles were collected and flash frozen in liquid nitrogen for LC-MS and GC-MS analysis of metabolites by the University of Michigan Metabolomics Core Facility, as detailed in the Supplemental Experimental Procedures.

Chronic Exercise

WT and AR113Q mice were run on an Exer3/6 treadmill (Columbus Instruments) from 8 to 14 weeks of age for 30 min per day, 5 days per week, at 10-m/min fixed speed. Control mice were placed on an immobile treadmill apparatus for the same amount of time. To analyze exercise capacity, a protocol for treadmill running was used as previously described (Chua et al., 2015). In brief, mice underwent 2 days of training on a treadmill, with day 1 consisting of 5 min of running at 8 m/min and day 2 consisting of 5 min of running at 8 m/min followed by 5 min at 10 m/min. On day 3, mice ran using a graded protocol consisting of 10 m/min for 40 min, then increasing speed by increments of 1 m/min every 10 min for a total of 30 min. This was followed by increasing speed at increments of 1 m/min every 5 min until mice were exhausted. Exhaustion was defined as mice making no attempt to exercise for 5 s. Distance run and time to exhaustion were recorded. At the end of the 6-week training period, body weight (g) and forelimb grip strength (g) were also measured.

Immunoprecipitation and Western Blotting

Quadriceps muscles were homogenized in RIPA buffer containing one tablet per 10 ml Complete Mini-Protease Inhibitor Mix (Roche), rotated for 2 hr at 4°C, and centrifuged at 13,000 × *g* for 10 min at 4°C. The supernatant fraction (500 μg) was incubated on a rotator overnight at 4°C with 10 μL AR antibody (Millipore, PG-21) or nonimmune rabbit immunoglobulin G (IgG) (Santa Cruz Biotechnology). Prewashed protein A-agarose beads (20 μL, Santa Cruz) were added, and samples were incubated for one additional hour at 4°C. Protein-antibody-bead complexes were washed six times in RIPA buffer in filtered spin columns (Thermo Fisher Scientific), and proteins were eluted by boiling in SDS-loading buffer for 5 min at 100°C. Samples were then resolved on a 7.5% SDS-PAGE gel.

Immunofluorescence Staining

Quadriceps and soleus/gastrocnemius muscles were placed on cork and embedded in OCT (optimal cutting temperature) compound (Tissue-Tek) immediately after collection. Cryosections were prepared using a Cryocut 1800 cryostat (Leica Biosystems) at 10 μm and placed on Superfrost Plus Microscope Slides (Thermo Fischer Scientific). Briefly, slides were incubated in acetone for 10 min, non-specific binding was blocked for 30 min at 37°C with 5% donkey serum in PBS-T (Tween 0.1% in PBS), and samples were incubated overnight at 4°C with the indicated antibodies in 1.5% donkey serum in PBS-T. Fluorescent secondary antibody was then applied for 1 hr at 37°C in 1.5% donkey serum in PBS-T. Basement membrane was stained with wheat germ agglutinin (WGA; green) at 5 μg/mL in PBS for 10 min at room temperature (RT). The slides were mounted using Vectashield with DAPI (Vector Laboratories) and sealed with nail polish. Muscle fiber size was measured by ImageJ (n = 4 mice per group, ≥25 fibers per mouse).

Antibodies

The following antibodies were used: anti-AR (PG-21, Merck Millipore; N20, Santa Cruz), anti-GAPDH (6C5, Novus Biologicals), type I/slow-twitch heavy-chain myosin (A4.840, DSHB, University of Iowa), and type II/fast-twitch heavy-chain myosin (Ab-2, Thermo Fisher Scientific). Horseradish peroxidase-conjugated secondary antibodies used for western blot analysis were from Bio-Rad. Goat anti-mouse IgG Alexa Fluor 555, goat anti-rabbit Alexa 488, and wheat germ agglutinin Alexa 488 conjugate antibodies used for immunofluorescence were from Life Technologies. Fluorescein isothiocyanate (FITC)-conjugated donkey anti-mouse IgM was from Jackson ImmunoResearch Laboratories.

Statistics

Data were analyzed using unpaired two-tailed Student's t test or one-way ANOVA with Newman-Keuls multiple comparison test in Prism 4 (GraphPad). Statistical significance was considered at $p < 0.05$. Low-rank thin-plate splines were used to estimate the curves of energy expenditure and VO_2 over time (Ruppert and Wand, 2003). The model includes a random effect for the intercept to account for correlations between measurements on the same subject. At a time point, comparisons between groups (WT versus AR113Q mice) were made using posterior distributions of the estimated outcome (such as VO_2) for each group. Statistical significance was determined by a 95% credible set for the difference. If the credible set does not include zero, the difference is statistically significant. WinBUGS (Version 1.4) was used for the analysis.

ACCESSION NUMBERS

The accession number for the RNA-seq data reported in this paper is GEO: GSE60691.

SUPPLEMENTAL INFORMATION

Supplemental Information includes Supplemental Experimental Procedures, five figures, and four tables and can be found with this article online at http://dx.doi.org/10.1016/j.celrep.2016.08.084.

AUTHOR CONTRIBUTIONS

E.G., Z.Y., J.P.C., and R.S. performed experiments. L.Z., F.Z., and Y.G. performed statistical analysis. S.V., M.P., G.H., and A.P.L. planned experiments and interpreted data. G.H. supplied essential reagents. E.G. and A.P.L. wrote the paper.

ACKNOWLEDGMENTS

We thank Dr. Mark Schultz for help with figure preparation. Work in this project utilized services from the University of Michigan Metabolomics Core and the University of Michigan Microscopy and Image Analysis Laboratory. This work was supported by grants from the NIH (R21 NS089516 and R01 NS055746 to A.P.L. and U24 DK097153 to the University of Michigan Metabolomics Core) and Telethon-Italy and Provincia Autonoma di Trento (TCP12013 to M.P.). G.H. is an employee of Ionis Pharmaceuticals. Ionis provided antisense oligonucleotides that were used in this study.

Received: December 18, 2015
Revised: July 5, 2016
Accepted: August 24, 2016
Published: September 27, 2016

REFERENCES

Atsuta, N., Watanabe, H., Ito, M., Banno, H., Suzuki, K., Katsuno, M., Tanaka, F., Tamakoshi, A., and Sobue, G. (2006). Natural history of spinal and bulbar muscular atrophy (SBMA): a study of 223 Japanese patients. Brain *129*, 1446–1455.

Chamberlain, N.L., Driver, E.D., and Miesfeld, R.L. (1994). The length and location of CAG trinucleotide repeats in the androgen receptor N-terminal domain affect transactivation function. Nucleic Acids Res. *22*, 3181–3186.

Chao, L.C., Zhang, Z., Pei, L., Saito, T., Tontonoz, P., and Pilch, P.F. (2007). Nur77 coordinately regulates expression of genes linked to glucose metabolism in skeletal muscle. Mol. Endocrinol. *21*, 2152–2163.

Chao, L.C., Wroblewski, K., Zhang, Z., Pei, L., Vergnes, L., Ilkayeva, O.R., Ding, S.Y., Reue, K., Watt, M.J., Newgard, C.B., et al. (2009). Insulin resistance and altered systemic glucose metabolism in mice lacking Nur77. Diabetes *58*, 2788–2796.

Chua, J.P., and Lieberman, A.P. (2013). Pathogenic mechanisms and therapeutic strategies in spinobulbar muscular atrophy. CNS Neurol. Disord. Drug Targets *12*, 1146–1156.

Chua, J.P., Reddy, S.L., Merry, D.E., Adachi, H., Katsuno, M., Sobue, G., Robins, D.M., and Lieberman, A.P. (2014). Transcriptional activation of TFEB/ZKSCAN3 target genes underlies enhanced autophagy in spinobulbar muscular atrophy. Hum. Mol. Genet. *23*, 1376–1386.

Chua, J.P., Reddy, S.L., Yu, Z., Giorgetti, E., Montie, H.L., Mukherjee, S., Higgins, J., McEachin, R.C., Robins, D.M., Merry, D.E., et al. (2015). Disrupting SUMOylation enhances transcriptional function and ameliorates polyglutamine androgen receptor-mediated disease. J. Clin. Invest. *125*, 831–845.

Cortes, C.J., Ling, S.C., Guo, L.T., Hung, G., Tsunemi, T., Ly, L., Tokunaga, S., Lopez, E., Sopher, B.L., Bennett, C.F., et al. (2014). Muscle expression of mutant androgen receptor accounts for systemic and motor neuron disease phenotypes in spinal and bulbar muscular atrophy. Neuron *82*, 295–307.

Dahlqvist, J.R., and Vissing, J. (2016). Exercise therapy in spinobulbar muscular atrophy and other neuromuscular disorders. J. Mol. Neurosci. *58*, 388–393.

Desport, J.C., Torny, F., Lacoste, M., Preux, P.M., and Couratier, P. (2005). Hypermetabolism in ALS: correlations with clinical and paraclinical parameters. Neurodegener. Dis. *2*, 202–207.

Huang, D.C., and Strasser, A. (2000). BH3-only proteins-essential initiators of apoptotic cell death. Cell *103*, 839–842.

Iacono, G., Altafini, C., and Torre, V. (2013). Early phase of plasticity-related gene regulation and SRF dependent transcription in the hippocampus. PLoS ONE *8*, e68078.

Jin, W., Goldfine, A.B., Boes, T., Henry, R.R., Ciaraldi, T.P., Kim, E.Y., Emecan, M., Fitzpatrick, C., Sen, A., Shah, A., et al. (2011). Increased SRF transcriptional activity in human and mouse skeletal muscle is a signature of insulin resistance. J. Clin. Invest. *121*, 918–929.

Johansen, J.A., Yu, Z., Mo, K., Monks, D.A., Lieberman, A.P., Breedlove, S.M., and Jordan, C.L. (2009). Recovery of function in a myogenic mouse model of spinal bulbar muscular atrophy. Neurobiol. Dis. *34*, 113–120.

Kanzleiter, T., Wilks, D., Preston, E., Ye, J., Frangioudakis, G., and Cooney, G.J. (2009). Regulation of the nuclear hormone receptor nur77 in muscle: influence of exercise-activated pathways in vitro and obesity in vivo. Biochim. Biophys. Acta *1792*, 777–782.

Kanzleiter, T., Preston, E., Wilks, D., Ho, B., Benrick, A., Reznick, J., Heilbronn, L.K., Turner, N., and Cooney, G.J. (2010). Overexpression of the orphan receptor Nur77 alters glucose metabolism in rat muscle cells and rat muscle in vivo. Diabetologia *53*, 1174–1183.

Katsuno, M., Adachi, H., Kume, A., Li, M., Nakagomi, Y., Niwa, H., Sang, C., Kobayashi, Y., Doyu, M., and Sobue, G. (2002). Testosterone reduction prevents phenotypic expression in a transgenic mouse model of spinal and bulbar muscular atrophy. Neuron *35*, 843–854.

Kazemi-Esfarjani, P., Trifiro, M.A., and Pinsky, L. (1995). Evidence for a repressive function of the long polyglutamine tract in the human androgen receptor: possible pathogenetic relevance for the (CAG)n-expanded neuronopathies. Hum. Mol. Genet. *4*, 523–527.

Kemp, M.Q., Poort, J.L., Baqri, R.M., Lieberman, A.P., Breedlove, S.M., Miller, K.E., and Jordan, C.L. (2011). Impaired motoneuronal retrograde transport in two models of SBMA implicates two sites of androgen action. Hum. Mol. Genet. *20*, 4475–4490.

Koch, L.G., and Britton, S.L. (2001). Artificial selection for intrinsic aerobic endurance running capacity in rats. Physiol. Genomics *5*, 45–52.

Langmead, B., Trapnell, C., Pop, M., and Salzberg, S.L. (2009). Ultrafast and memory-efficient alignment of short DNA sequences to the human genome. Genome Biol. *10*, R25.

Lantier, L., Fentz, J., Mounier, R., Leclerc, J., Treebak, J.T., Pehmøller, C., Sanz, N., Sakakibara, I., Saint-Amand, E., Rimbaud, S., et al. (2014). AMPK controls exercise endurance, mitochondrial oxidative capacity, and skeletal muscle integrity. FASEB J. *28*, 3211–3224.

Lieberman, A.P., and Fischbeck, K.H. (2000). Triplet repeat expansion in neuromuscular disease. Muscle Nerve *23*, 843–850.

Lieberman, A.P., Harmison, G., Strand, A.D., Olson, J.M., and Fischbeck, K.H. (2002). Altered transcriptional regulation in cells expressing the expanded polyglutamine androgen receptor. Hum. Mol. Genet. *11*, 1967–1976.

Lieberman, A.P., Yu, Z., Murray, S., Peralta, R., Low, A., Guo, S., Yu, X.X., Cortes, C.J., Bennett, C.F., Monia, B.P., et al. (2014). Peripheral androgen receptor gene suppression rescues disease in mouse models of spinal and bulbar muscular atrophy. Cell Rep. *7*, 774–784.

Mailloux, R.J., and Harper, M.E. (2012). Mitochondrial proticity and ROS signaling: lessons from the uncoupling proteins. Trends Endocrinol. Metab. *23*, 451–458.

Maxwell, M.A., Cleasby, M.E., Harding, A., Stark, A., Cooney, G.J., and Muscat, G.E. (2005). Nur77 regulates lipolysis in skeletal muscle cells. Evidence for cross-talk between the beta-adrenergic and an orphan nuclear hormone receptor pathway. J. Biol. Chem. *280*, 12573–12584.

Mhatre, A.N., Trifiro, M.A., Kaufman, M., Kazemi-Esfarjani, P., Figlewicz, D., Rouleau, G., and Pinsky, L. (1993). Reduced transcriptional regulatory competence of the androgen receptor in X-linked spinal and bulbar muscular atrophy. Nat. Genet. *5*, 184–188.

Monks, D.A., Johansen, J.A., Mo, K., Rao, P., Eagleson, B., Yu, Z., Lieberman, A.P., Breedlove, S.M., and Jordan, C.L. (2007). Overexpression of wild-type androgen receptor in muscle recapitulates polyglutamine disease. Proc. Natl. Acad. Sci. USA *104*, 18259–18264.

Overmyer, K.A., Thonusin, C., Qi, N.R., Burant, C.F., and Evans, C.R. (2015). Impact of anesthesia and euthanasia on metabolomics of mammalian tissues: studies in a C57BL/6J mouse model. PLoS ONE *10*, e0117232.

Palamiuc, L., Schlagowski, A., Ngo, S.T., Vernay, A., Dirrig-Grosch, S., Henriques, A., Boutillier, A.L., Zoll, J., Echaniz-Laguna, A., Loeffler, J.P., and René, F. (2015). A metabolic switch toward lipid use in glycolytic muscle is an early pathologic event in a mouse model of amyotrophic lateral sclerosis. EMBO Mol. Med. *7*, 526–546.

Palazzolo, I., Stack, C., Kong, L., Musaro, A., Adachi, H., Katsuno, M., Sobue, G., Taylor, J.P., Sumner, C.J., Fischbeck, K.H., and Pennuto, M. (2009). Overexpression of IGF-1 in muscle attenuates disease in a mouse model of spinal and bulbar muscular atrophy. Neuron *63*, 316–328.

Pearen, M.A., and Muscat, G.E. (2010). Minireview: Nuclear hormone receptor 4A signaling: implications for metabolic disease. Mol. Endocrinol. *24*, 1891–1903.

Querin, G., Bertolin, C., Da Re, E., Volpe, M., Zara, G., Pegoraro, E., Caretta, N., Foresta, C., Silvano, M., Corrado, D., et al.; Italian Study Group on Kennedy's disease (2016). Non-neural phenotype of spinal and bulbar muscular atrophy: results from a large cohort of Italian patients. J. Neurol. Neurosurg. Psychiatry *87*, 810–816.

Ramzan, F., McPhail, M., Rao, P., Mo, K., Halievski, K., Swift-Gallant, A., Mendoza-Viveros, L., Cheng, H.Y., and Monks, D.A. (2015). Distinct etiological roles for myocytes and motor neurons in a mouse model of Kennedy's disease/spinobulbar muscular atrophy. J. Neurosci. *35*, 6444–6451.

Ranganathan, S., Harmison, G.G., Meyertholen, K., Pennuto, M., Burnett, B.G., and Fischbeck, K.H. (2009). Mitochondrial abnormalities in spinal and bulbar muscular atrophy. Hum. Mol. Genet. *18*, 27–42.

Rhodes, L.E., Freeman, B.K., Auh, S., Kokkinis, A.D., La Pean, A., Chen, C., Lehky, T.J., Shrader, J.A., Levy, E.W., Harris-Love, M., et al. (2009). Clinical features of spinal and bulbar muscular atrophy. Brain *132*, 3242–3251.

Rocchi, A., Milioto, C., Parodi, S., Armirotti, A., Borgia, D., Pellegrini, M., Urciuolo, A., Molon, S., Morbidoni, V., Marabita, M., et al. (2016). Glycolytic-to-oxidative fiber-type switch and mTOR signaling activation are early-onset features of SBMA muscle modified by high-fat diet. Acta Neuropathol. *132*, 127–144.

Ruppert, D., Wand, M.P., and Carroll, R.J. (2003). Semiparametric Regression (Cambridge University Press).

Shrader, J.A., Kats, I., Kokkinis, A., Zampieri, C., Levy, E., Joe, G.O., Woolstenhulme, J.G., Drinkard, B.E., Smith, M.R., Ching, W., et al. (2015). A randomized controlled trial of exercise in spinal and bulbar muscular atrophy. Ann. Clin. Transl. Neurol. *2*, 739–747.

Sorarù, G., D'Ascenzo, C., Polo, A., Palmieri, A., Baggio, L., Vergani, L., Gellera, C., Moretto, G., Pegoraro, E., and Angelini, C. (2008). Spinal and bulbar muscular atrophy: skeletal muscle pathology in male patients and heterozygous females. J. Neurol. Sci. *264*, 100–105.

Takeyama, K., Ito, S., Yamamoto, A., Tanimoto, H., Furutani, T., Kanuka, H., Miura, M., Tabata, T., and Kato, S. (2002). Androgen-dependent neurodegeneration by polyglutamine-expanded human androgen receptor in Drosophila. Neuron *35*, 855–864.

Trapnell, C., Pachter, L., and Salzberg, S.L. (2009). TopHat: discovering splice junctions with RNA-Seq. Bioinformatics *25*, 1105–1111.

Trapnell, C., Hendrickson, D.G., Sauvageau, M., Goff, L., Rinn, J.L., and Pachter, L. (2013). Differential analysis of gene regulation at transcript resolution with RNA-seq. Nat. Biotechnol. *31*, 46–53.

Villena, J.A. (2015). New insights into PGC-1 coactivators: redefining their role in the regulation of mitochondrial function and beyond. FEBS J. *282*, 647–672.

Yu, Z., Dadgar, N., Albertelli, M., Gruis, K., Jordan, C., Robins, D.M., and Lieberman, A.P. (2006a). Androgen-dependent pathology demonstrates myopathic contribution to the Kennedy disease phenotype in a mouse knock-in model. J. Clin. Invest. *116*, 2663–2672.

Yu, Z., Dadgar, N., Albertelli, M., Scheller, A., Albin, R.L., Robins, D.M., and Lieberman, A.P. (2006b). Abnormalities of germ cell maturation and Sertoli cell cytoskeleton in androgen receptor 113 CAG knock-in mice reveal toxic effects of the mutant protein. Am. J. Pathol. *168*, 195–204.

Yu, Z., Wang, A.M., Adachi, H., Katsuno, M., Sobue, G., Yue, Z., Robins, D.M., and Lieberman, A.P. (2011). Macroautophagy is regulated by the UPR-mediator CHOP and accentuates the phenotype of SBMA mice. PLoS Genet. *7*, e1002321.